Analysis of false alarm for imaging space-based laser warning system

DONG Hong-jun(董红军)*, **ZHOU Zhong-liang**(周中亮), **and HUANG Fu-yu**(黄富瑜)
Department of Optics and Electronic Engineering, Ordnance Engineering College, Shijiazhuang 050003, China

(Received 9 September 2011)

In view of the problem of false alarm in imaging space-based laser warning system, the effects of sunlight and lightning on the threaten laser detection and attack event determination are studied by analyzing and calculating the radiant energy density and space-time feature of imaging spot, respectively. The results show that the main false alarm resourses of space-based laser warning system are sunlight and lightning. The sunlight should exposure the detector directly in one ninth of the satillite orbital period, and the imaging spot of sun is similar to the attack laser. The lightning imaging spot is similar to the illumination laser. About 1.4 lightning events can occur in the field of view (FOV) of the warning system per second. It could not discriminate spots of sun, lightning and threaten laser by the frame subtraction technology.
Document code: A **Article ID:** 1673-1905(2012)02-0105-4
DOI 10.1007/s11801-012-1070-y

With the development of military laser technology in modern war, the satellite faces more and more laser threats as the appearance of anti-satellite laser weapon[1-3]. Therefore, it is important to study the satellite protection technology in order to limit or avoid the threat. Space-based laser warning system is the basic countermeasure which can detect and recognize threaten lasers to assess their threat level and plan avoidance or retaliation. Since the space-based laser warning system which is installed on the satellite has a large field of view (FOV), the detection of threaten laser is easily interfered by the background radiation. Thus, the false alarm is a serious problem which must be investigated and solved.

Some researches have been done regarding the false alarm rejection of laser warning system. But the studies usually focused on the detector noise and background noise[4-6]. However, the power of threaten laser, which is detected by space-based laser warning system, is much higher than that of the laser objected by other typical laser warning systems, such as ranging laser and riding laser. Since the signal noise ratio (SNR) of imaging spot of threaten laser is above 30 dB, the noise and stray light can not induce false alarm[7]. Although the irradiance intensity of background is greater than that from the ground warning system, it can be suppressed effectively by frame subtraction technology, as the background is temporally steady. But some natural phenomena, such as sunlight and lightning, can trigger threat reports if they match the characteristics of threaten lasers in the waveband of the warning system[8]. Therefore, it is necessary to analyze the characteristics of these radiation sources.

Typically, the imaging laser warning system consists of a front-end optical assembly, a narrow-band filter, a CCD focal plane array assembly with drive electronics and a developed operation and signal processing module for the identifying and orientation of threaten lasers. The system structure is shown in Fig.1.

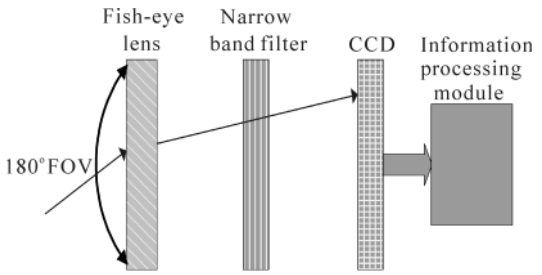

Fig.1 Schematic diagram for laser warning system

The optics detector consists of an *f*/0.5 infrared fish-eye lens assembly with the aperture of 1.2 mm, the focal length of 2.4 mm and the field angle of 180°×180°. The principal axis orientates to the geocenter. A narrow-band filter with central wavelength of 1.315 μm is used to suppress the background light out of band. The focal plane array assembly consists of a near infrared CCD array with the resolution of 320 pixel × 256 pixel and the pixel pitch of 30 μm × 30 μm. The responsive bandwidth of CCD ranges from 0.9 μm

* E-mail:dhjoptics@126.com

to 1.7 μm. Each image scene is integrated in 2 ms.

The total visible sector of the warning system on the earth can be expressed as

$$\alpha = 2\arcsin\frac{R_e}{R_e + R_h} , \quad (1)$$

where R_h denotes the satellite orbital altitude, and R_e denotes the radius of earth. The geographical coverage of the system is shown as the dashed area in Fig.2, and it can be calculated as

$$S = 2\pi R_e^2\left(1-\cos(\frac{\pi-\alpha}{2})\right) . \quad (2)$$

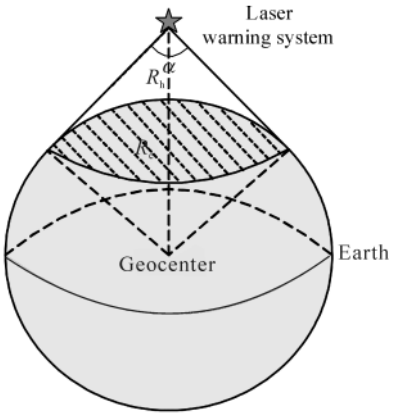

Fig.2 Schematic diagram for FOV of the laser warning system

We take the MSTI-3 satellite of US for example, whose orbital altitude is 420 km, running speed is 7.6 km/s, and orbital period is 5618 s. It can be calculated that the total visible sector on the earth is 139.6° and the geographical coverage of system is 1.58×10^7 km^2. The geographical coverage of each pixel is 13.9 km × 13.9 km, and the angular displacement of each frame image is $(1.28\times10^{-4})°$. Hence, the background of the adjacent frame image is considered to be steady.

To analyze the effects of the interference radiation sources on the detection and identifying of the threaten laser, the characteristics of imaging spots of threaten laser, sunlight and lightning are investigated, respectively.

Because the divergence angle of laser beam is smaller, and the diameter of the laser beam expands to more than 1 m to reduce the effect of atmospheric turbulence when the beam carries energy over kilometers through the atmosphere, the diameter of laser beam in the satellite is much larger than the aperture of fish-eye lens. The laser beam projected onto a CCD chip through the lens can be imaged into a small blur spot as the parallel light.

Owing to the shorter focal length of fish-eye lens, which is usually only a few millimeters to ten millimeters, the diameter of imaging spot is only several microns in the focal plane. The spot size is determined by diffraction, atmospheric turbulence and optical aberration of fish-eye lens. For our system, the diameter of spot is about 26.5 μm for normal incidence[7]. When the energy of the threaten laser is high, the central pixel can be saturation. The spot size becomes larger due to the blooming effects.

To demonstrate the imaging spot of threaten laser detected by warning system, we perform some experiments with commercial available components. A 1.315 μm CW solid laser source with projection radius of 1 mm, adjustable power of 0 −1 W and beam divergence angle of 1.5 mrad, combined with extending collimating lens is used to simulate threaten laser. Fig.3 shows the imaging spots of threaten laser for different laser intensities and incident angles recorded by the detector.

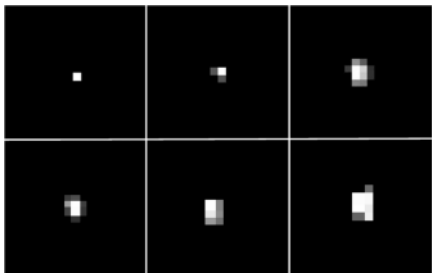

Fig.3 Focusing laser spots for different laser intensities and incident angles

The threaten laser includes two kinds[9]. One is the illumination laser which is used for aiming and ranging before attacking. Because the illumination laser is pulse laser with the energy density on the satellite about 10^{-1} μJ/cm^2, it can only be recorded by one frame image. The other is the attack laser which is CW laser commonly with the energy density of 10 mW/cm^2–10 W/cm^2. The attack laser should sustain several ten seconds to achieve blinding or even damaging. The attack laser can be detected by serial frame images. In our system, the angular resolutions are 0.8° in 0° field angle and 4° in 90° field angle. Because the angular motion of attack laser is smaller, the imaging spots are located on the same position for serial images.

Commonly, the space-based detector can avoid the direct sunlight exposure because of the small FOV and baffle. But for the 180° FOV of fish-eye lens, the effects of direct sunlight exposure on the detector of warning system would not be avoided. The relative positions of sun, earth and laser warning system are illustrated in Fig.4.

When the satellite travels in the orbital region of $\angle A$, both the direct sunlight and reflected sunlight can not irradiate the detector, as the sun is obstructed by earth entirely. In the orbital region of $\angle B$, the direct sunlight could not irradiate the detector, as the back of detector faces the sun.

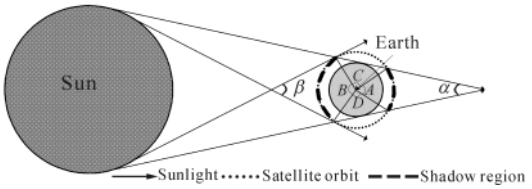

Fig.4 Schematic diagram for relative positions of sun and laser warning system

However, the direct sunlight should irradiate the detector in the orbital regions of $\angle C$ and $\angle D$. According to the geometrical relationship, it can be obtained as

$$\sin\frac{\alpha}{2}=\frac{R_s-R_e}{R_{se}}, \tag{3}$$

$$\sin\frac{\beta}{2}=\frac{R_s+R_e+R_h}{R_{se}}, \tag{4}$$

where R_s and R_e are the radii of sun and earth, respectively, R_h is the satellite orbital height and R_{se} is the solar-earth distance. It can be calculated that α=9.22 mrad, β = 9.44 mrad, $\angle A$ =138.6°, $\angle B$ =179.5° and $\angle C = \angle D$ =20.9°.

Thus, the direct sunlight could irradiate the detector in one ninth of the orbital period. At such a long distance as 1 AU, the sun effectively behaves like a point source, and the diffraction-limited system produces an Airy disk. The angular radius of sun imaged on the detector can be written as

$$\phi=\sqrt{\sigma_d^{\,2}+\sigma_a^{\,2}+(\varphi/2)^2}=7.22 \ \text{mrad}, \tag{5}$$

where φ is the average field angle of sun in the satellite position, σ_a is the aberration factor, and σ_d is the diffusion factor. The diameter of imaging spot is given by

$$d_s=2f\cdot\phi=34.7\ \mu\text{m} \quad . \tag{6}$$

Therefore, the irradiance of direct sunlight at the entrance pupil of the detector can be written as[10]

$$W_{ss}=\int_{\lambda_1}^{\lambda_2}\frac{c_1}{\lambda^5}\cdot\frac{1}{\exp(c_2/\lambda T)-1}\cdot\left(\frac{R_{se}}{R_s}\right)^2\cos\theta\,\mathrm{d}\lambda, \tag{7}$$

where λ_1 and λ_2 are the lower and upper limits of the spectral band for warning system, T is the black-body temperature of the sun, θ is the zenith angle, and c_1, c_2 are the radiometric constants.

Neglecting the effects of asymmetrical distribution of the energy within Airy disk, the power density of imaging spot can be represented by

$$W_D=W_{ss}S_D\tau_t\tau_f/S_s, \tag{8}$$

where S_D is the entrance pupil area, τ_t is the spectral transmissivity of system, τ_f is the transmissivity of filter, and S_s is the area of sun spot.

In the orbital region where the direct sunlight exposures the detector, the zenith angle of sun is varied from 69° to 90°. The imaging spots of sun recorded by warning system in ground experiments are shown in Fig.5.

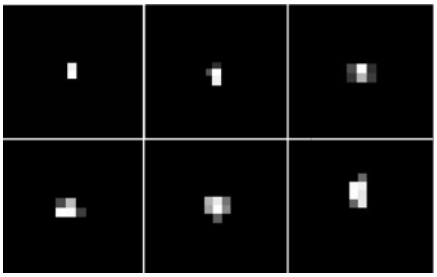

Fig.5 Solar spots recorded by warning system for different solar zenith angles

It can be found that the imaging spot of sun is similar to the threaten laser in profile and size. Considering the attenuation of aerosphere, the spot recorded in the satellite can be larger than that recorded on the ground due to higher solar irradiance.

When the satellite travels from orbit regions of $\angle A$, $\angle B$ to regions of $\angle C$, $\angle D$ in Fig.4, the sun spot can be imaged on the focal plane. Because the angular displacement from sun to satellite in the integrate time is much less than the angular resolution of one CCD pixel, the position of sun spot is fixed in CCD plane for serial images. Since the imaging spots of sun and laser are similar in temporal and spatial domains, it is difficult to recognize the threaten laser in term of time-space characteristics.

While the optical energy of lightning discharge ranges from radio frequency to X-ray, its energy is stronger in the near-infrared spectrum. The median peak power and median detected optical energy of a lightning flash are estimated to be 10^9 W and 4.5 × 10^5 J, respectively[11]. Generally, one lightning includes several flashes, and each flash sustains about 500 μs. For the majority (about 90%) of the lightning discharges, the peak radiances are larger than 4.7 μJ•m^{-2}•sr^{-1}. The energy is radiated from the luminous part of the lightning channel, and then subjected to multiple scatterings within the cloud. The emitted optical energy is transferred from a line source to a surface source, and finally the cloud surface is illuminated. Monte Carlo simulations and observations from aircraft and space shuttle show a distribution of the optical energy over an area of approximately 10 km in diameter, and 40 km for the biggest[12,13].

The fraction of energy scattered from the top of cloud into space can be detected by infrared detector. The height of lightning cloud layer is about 10 km on average. The lightning can be regarded as a point source, because the distance from lightning to detector is much larger than the size of cloud cluster. It can be estimated that the diameters of imaging spots are 10 − 60 μm for different incident angles and distances. The power density of lightning emitted upward is approximately

10^{-7} J•nm^{-1}•m^{-2}•sr^{-1} in infrared band. The average power density of lightning in the entrance pupil of detector is a little larger than that of the illumination laser.

The first systematic study of spatially resolved terrestrial lightning flashes from space started with the lightning imaging sensor (LIS)[13]. The system works in near infrared band. The pixel pitch is 13 μm × 13 μm, corresponding to the area of 12.5 km^2. Fig.6 shows the images of the flashes recorded over South Africa.

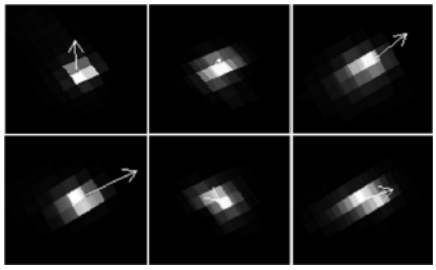

Fig.6 Individual terrestrial flashes observed by LIS over South Africa

The brightness distributions are projected onto the horizontal plane on the earth. The size and shape of these flashes are typical for other locations. The flash image in each 50 km × 50 km box is produced by accumulating the intensity of the 2 ms LIS frames during an approximately 0.5 s single flash. The flash in each box is projected onto the horizontal plane on the earth. The arrows point toward the spacecraft. The length of the arrows shows the emission angle.

Since the duration time of lightning is less than the integration time of CCD, the lightning could be recorded by only one image. Comparing Fig.3 with Fig.6, it can be found that the small diffuse lightning spots are more analogous than the laser spots. It is a serious interference to the identification of illumination laser.

According to the recent measurement, the global lightning flash rate is approximately 50 s^{-1}[14]. To the flash rate, about 1.4 lightning events per second can be expected in the FOV of warning system on average. It is a frequent interference to the detector, as the false alarm rate achieves 10^{-2} for our system.

The characteristics of imaging spots of threaten laser, sun and lightning are studied by numerical calculation and experimental analysis. As the imaging spot features of the sun and attack laser, lightning and illumination laser are similar in time, space and intensity, the warning system could not distinguish the threaten laser and the false targets. The direct sunlight can exposure the detector in one ninth of the satellite orbital period, and about 1.4 lightning events per second can be expected in the FOV of warning system. Unless advanced laser detection technology and false alarm rejection algorithm are used, the warning system can not operate normally. In addition, launching rocket, falling meteor, spacecraft with larger reflecting surface and other objects may also induce false alarms. Fortunately, they can be ignored as the smaller probability.

References

[1] J. Dubois and F. Reid, Detecting Laser Sources on the Battlefield, Ottawa, Proc. SPIE **6792**, 67962F (2007).

[2] Alastair D. McAulay, Detecting Modulated Lasers in the Battlefield and Determining Their Direction, Orlando, Proc. SPIE **7336**, 73361J (2009).

[3] Dave H. Hillanf, Gary S. Phippset and Curt M. Jingle, Satellite Threat Warning and Attack Reporting, IEEE Aerospace Conference **2**, 207 (1998).

[4] Donald W. Wilmot, William R. Owens and Robert J. Shelton, The Infrared and Electro-Optical Systems Handbook, SPIE Optical Engieering Press, 77 (1993).

[5] YU Lei, LIN Guan-yu, QU Yi and WANG Shu-rong, Journal of Optoelectronics • Laser **22**, 42 (2011). (in Chinese)

[6] KONG Ying-ying, ZHOU Jian-jiang and ZHANG Yan, Journal of Optoelectronics • Laser **21**, 1257 (2010). (in Chinese)

[7] DONG Hong-jun, ZHOU Zhong-liang and HUANG Fu-yu, Optical Technique **37**, 376 (2011). (in Chinese)

[8] DONG Hong-jun and ZHOU Zhong-liang, Acta Photonica Sinica **40**, 388 (2011). (in Chinese)

[9] LI Fa-quan, CHENG-Xuewu, YANG Yong, LI Xiao-yin and GONG Shun-sheng, Infrared and Laser Engineering **37**, 331 (2008). (in Chinese)

[10] ZHANG Hai-hong, WANG Jian-yu, SHU Rong and HU Yi-hua, J. Infrared Millim. Waves **25**, 426 (2006). (in Chinese)

[11] T. E. Light, D. M. Suszcynsky, M. W. Kirkland and A. R. Jacobson, J. Geophys. Res. **106**, 17103 (2001).

[12] H. J. Christian, R. J. Blakeslee and S. J. Goodman, J. Geophys. Res. **94**, 13329 (1989).

[13] D. J. Boccippio, W. J. Koshak and R. J. Blakeslee, J. Atmos. Oceanic Technol. **19**, 1318 (2002).

[14] Hugh J. Christian, Richard J. Blakeslee, Dennis J. Boccippio, William L. Boeck, Dennis E. Buechler, Kevin T. Driscoll, Steven J. Goodman, John M. Hall, William J. Koshak, Douglas M. Mach and Michael F. Stewart, J. Geophys. Res. **108**, 4005 (2003).